# CHAPTER II

CORRELATION OF SOL-GEL PROCESSING PARAMETERS WITH MICROSTRUCTURE AND PROPERTIES OF CERAMIC PRODUCT

Abstract

Very high purity $MgAl_2O_4$ spinel precursor can be prepared via the low temperature process called "Oxide One Pot Synthesis Process, (OOPS)". Sol-gel processing of such precursors offers the opportunity to prepare spinels with controlled microstructures, which is key to optimizing their properties for application as humidity sensors. Sol-gel processing of a double alkoxide precursor was carried out in buffer solutions in the range pH 8-12, to investigate the effect on the physical properties of the sintered ceramic products The structure and morphology of the latter were characterized using FTIR, XRD, SEM and BET surface area measurements. Sol-gel processing results in a sintered product with narrow pore size distribution and containing a spinel phase of high crystallinity. At higher pH values, increasing amounts of an α-Al_2O_3 phase are formed. At all pH values, the sintered product exhibits high water adsorption, up to 0.312 g H_2O/g sample.

Introduction

MgAl$_2$O$_4$ is a well-known mineral used as a refractory material in the ceramic industry. The MgAl$_2$O$_4$ precursor can be prepared via chemical reaction using an inexpensive preceramic precursor synthesized directly from the metal oxide or alkoxide. Chemical routes offer many advantages over traditional methods, including the potential to control product homogeneity and purity, to lower processing temperatures, and to control the size, shape, and distribution of the resulting ceramic particles, increasingly necessary for producing advanced ceramics. One of the simplest chemical processes, called the "Oxide One Pot Synthesis Process" (OOPS) can produce oligomeric precursors containing any combination of Al, Si, and group I or II metals in one step.[1-3] The preparation of a spinel double alkoxide precursor is based on the following reaction:

$$2Al(OH)_3 + MgO + 3TEA + x'EG \longrightarrow Spinel\ Precursor \quad (1)$$
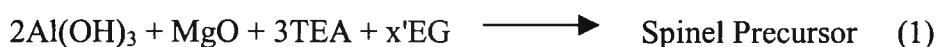
The spinel, MgAl$_2$O$_4$, is a pure ceramic material that has many applications. The one of interest here is a ceramic humidity sensor with better chemical resistance and mechanical strength than polymeric sensors. The ceramic sensors are based on a porous sintered oxide. Many types have been studied and prototype devices developed which make use of the unique electrical properties of these materials.[4-7] It is well known that the electrical properties of ceramic materials are sensitively related to their microstructure. The presence of a large pore volume is considered as fundamental for ceramic materials used in humidity sensors. Modification of the chemical composition and microstructure of ceramic materials by changing parameters in the production process permits both performance optimizations in devices exploiting the electrical properties of ceramics and tailoring of the device to specific applications.

Sol-gel processing, which can be carried out at ambient conditions and is inexpensive compared to other techniques, has been extensively used to prepare amorphous and crystalline ceramics. Different sol-gel routes to spinel formation have been explored, and the results show that sol-gel synthesis of a double alkoxide precursor allows pure spinel nanosized materials to be obtained[8]. Materials can be produced in a variety of forms, such as fine powders, thin films, monoliths and fiber. In addition, the sol-gel process offers the ability to change or control physical

characteristics such as pore size distribution and pore volume. However, to achieve such control, it is necessary to adjust the rate of hydrolysis and condensation reactions. In this paper we investigate the effect of such processing variables on the microstructure and properties of the ceramic products produced by hydrolysis of a spinel double alkoxide precursor.

Experimental

Materials

Aluminium hydroxide ($Al(OH)_3$) and magnesium oxide (MgO) were purchased from Sigma Chemical Co. and AJAX Chemicals, respectively. They were used as received. Triethanolamine (TEA, $N(CH_2CH_2OH)_3$, was supplied by Carlo Erba and used as received. Ethylene glycol (EG, $OHCH_2CH_2OH$) was obtained from J.T.Baker Inc. and distilled before use. Tri-sodium phosphate ($Na_3PO_4.12H_2O$), Citric acid ($HOOCCH_2C(OH)COOHCH_2COOH.H_2O$) and Boric acid ($H_3BO_3$) were obtained from Carlo Erba Reagents, APS Ajax Finechem and Merck, respectively.

Instrumental

Mass spectra were obtained using a FISONS Instruments 707 VG Auto spec-ultima mass spectrometer (Manchester, England) with a VG data system, using the positive fast atomic bombardment (FAB^+-MS) mode, employing a direct probe inlet and using the Cs gun to ionize the sample molecules. The peaks were calibrated using CsI as reference. The sample was mixed with glycerol, as matrix. The mass range of sample was set from m/z=20 to 3000. FTIR spectroscopic analysis was conducted using a Bruker Instrument (EQUINOX55) with a resolution of 4 cm^{-1}. The solid samples were prepared by mixing 1% of samples with anhydrous KBr, while the liquid samples were analyzed using a Zn-Se window cell. Thermal properties were analyzed by thermogravimetric analysis (TGA) using a Du Pont Instruments TGA 2950. The heating rate was 10^0C/min and the sample weight was 10-20 mg. The crystallinity of ceramic products was characterized by a Rigaku X-ray diffractometer at a scanning speed of 5 degree/sec using $CuK\alpha$ as source. The working range was 2θ = 5-80. SEM microscopy was performed using a JEOL 5200-2AE scanning electron microscope. Electron probe microanalysis (EPMA) was

applied to analyze samples using an X-ray mode detector (SEM/EDS). A fluid rheometer , model ARES, from Rheometric Scientific Inc., was used to determine the storage and loss shear moduli, $G'(\omega)$, $G''(\omega)$, and the dynamic viscosity, $\eta^*(\omega) = (G'^2 + G''^2)^{1/2}/\omega$ as a function of angular frequency, $\omega = 0.4$, 0.8, 1.6, 3.2, 6.4, 12.8 and 25.6 rad/s. A 50 mm. diameter cone and 0.04 radian angle was used, with a 10g transducer. The % strain was varied from 1-3%. The temperature was controlled using a circulating fluid bath. The sintering process was carried out using Carbolite Furnace (CSF 1200) and Carbolite (RHF 1600). The surface area was obtained using a Quantasorb JR. (Autosorb-1).

Synthesis of MgAl$_2$O$_4$ precursor

Preparation of the MgAl$_2$O$_4$ precursor followed previous work[2] specifically: Aluminium hydroxide (Al(OH)$_3$) [64-66% as Al$_2$O$_3$, 15.95 g, 100mmol], magnesium oxide (MgO) [96%asMgO,4.30 g,100mmol], and triethanolamine (TEA) [>99%, 40ml, 300mmol] were dissolved in 150 ml distilled EG. The mixture was added into a 250ml two-neck round bottom flask. It was then heated at 200°C to distill off EG and water (by- product) for 7 h under nitrogen atmosphere. The desired precursor was further distilled approximately 10 h. at 100°-150°C under vacuum (10^{-2} torr) to remove most of EG residue. The precursor obtained was identified using TGA, FTIR and FAB$^+$MS. The identified precursor was pyrolyzed at 400°-1200°C to form spinel. The sintered product was studied using FTIR, XRD and SEM.

Sol-Gel processing

The MgAl$_2$O$_4$ precursor was mixed with buffer solutions of pH 3-12 prepared by using the mixture of 0.2 M Boric acid, 0.05M Citric acid and 0.1M tri-sodium phosphate, at 27°C and with buffers of pH 8 and 9 at 40°C. The concentration used was 20% (w/v). After gel was formed and aged at room temperature, the gel was sintered at different temperatures to form ceramic product. The temperature used was varied from 400°-1300°C. Sintered products were characterized using FTIR, XRD, and BET, and subsequently, were tested for moisture adsorption

Sol-Gel transition of MgAl₂O₄

The spinel precursor, without purification, after removal of ethylene glycol, was used to investigate the sol-gel transition. The material was dissolved in buffer solutions of pH 8-12 at a concentration of 20%(w/v). The hydrolysis temperatures were ambient and 40°C. The solution was stirred until homogeneous, prior to being transferred to the rheometer for rheological analysis.

Characterization

The molecular structure of precursor and sintered gel were characterized by FTIR. The crystalline structure was characterised using XRD. The morphology of ceramic product from precursor and sintered gel was studied using SEM. Surface area, pore volume and pore size distribution was measured using the Autosorb-1. The kinetics of the sol-gel transition was studied using the fluid rheometer.

Results and Discussion

Precursor Synthesis

$MgAl_2O_4$ precursor was synthesized by Oxide-One-Pot-Synthesis process (OOPS). The product obtained was a yellow brittle solid. Because of the sensitivity to moisture, the obtained product was required to be stored under vacuum in a dessicator. The structure of the precursor was presumed to be the trimetallic species shown in fig.1. FAB^+-MS analysis showed the highest mass peak at m/e = 518, which is characteristic of the structure of precursor. The proportion of Al and Mg were obtained using EPMA, in EDS mode. The ratio of Al: Mg was determined to be equal to 1.99.

FTIR analysis of the precursor is shown in Fig.2. The peak position at 3000-3500 cm^{-1} is characteristic of H-bonded OH stretch. The peak position at 2900-3000 cm^{-1} corresponds to C-H stretch of methylene groups, and the broad peak at 650 cm^{-1} is assigned to Al-O-Mg bonds.

TGA analysis shows 3 regions of weight loss. The first region, at 220°-400°C, corresponds to organic ligand decomposition and generates a char as a product. The next region at 400°-600°C, is carbon residue decomposition. The final mass loss occurs between 600°-750°C and results from the decomposition of $MgCO_3$ formed

during organic ligand decomposition. The total % ceramic yield obtained was 25.94%, which was less than the theoretical yield, i.e. 27.47%. The reason is the presence of residual organic material, principally TEA

XRD analysis of the precursor indicates the evolution of microstructure on sintering at different temperatures as shown in Fig.3. All the peak positions were identified by comparison with JCPDS file No. 21-1152 ($MgAl_2O_4$, cubic structure). At sintering temperatures lower than 700°C, XRD shows only a broad peak, but on increasing temperature up to 700°C a diffraction pattern characteristic for a γ-Al_2O_3-$MgAl_2O_4$ solid solution is generated. The diffraction patterns of γ-Al_2O_3 and $MgAl_2O_4$ spinel are very similar: the major peaks of the spinel are the 311hkl reflection (d=0.244nm, I=100%) and the 400 hkl reflection (d= 0.202 nm., I = 60-65%), whereas the major peaks of γ-Al_2O_3 are the 400hkl (d=0198 nm., I= 100%) and the 311 reflections (d = 0.239 nm, I = 80%). These reflections overlap to give intense peaks at 2theta = 36.7 degrees and 2theta = 44.7 degrees. Using the method of Pasquire et al. [8] to follow the phase evolution, the relative intensity ratio of the 400 and 311 peaks was monitored until it remained constant. A ratio of I_{311}/I_{400} ~ 0.6-0.65 indicates the presence of pure $MgAl_2O_4$ spinel. A higher ratio indicates the spinel phase was a solid solution of γ-Al_2O_3 and $MgAl_2O_4$. Thus examining Fig. 3, we find that at 700-800°C, a solid solution of γ-Al_2O_3 and $MgAl_2O_4$ was formed, but at 1200°C, pure $MgAl_2O_4$ spinel was produced. A similar result was found in previous studies of spinel produced via the sol-gel process[8]. The presence of γ-Al_2O_3 at lower sintering temperatures is presumed[8] to reflect local compositional heterogeneities within the spinel phase, which arise during sol-gel processing because of preferential hydrolysis of one element (AL or Mg).

The SEM micrograph of the spinel precursor after sintering at 1200°C is shown in Fig 7a. The spinel contains irregularly shaped particles possibly because a high level of agglomeration occurs during the precursor pyrolysis. The specific surface area of the spinel precursor sintered at 1200°C is listed in Table I.

Sol-Gel processing

Varying the pH of the buffer solution in the range 3-12, for a concentration of 20% (W/V), we observed that gel formation was not as successful at acidic pH as

at basic pH. In acidic solution, gel forms at only a few pH values close to neutral, and the process took a very long time. On the other hand, in basic solution, gel formed over the entire range, albeit at gelation times which depend on pH.

FTIR analysis was used to follow the hydrolysis reaction of the precursor. As shown in Fig. 4, the spectrum of the gel during hydrolysis shows progressive increase of intensity at peak positions characteristic of Al-O-Al bonds at approximately 500-800 cm^{-1}. Al-O-Al bonds were formed by the hydrolysis reaction of the precursor. With increasing time the peak is not only more intense but is also sharper. The peak at 1000-1100 cm^{-1}, corresponding to C-O stretching of TEA also increases. This reflects that TEA was produced in the hydrolysis reaction. Comparing the spectra of gels formed in the pH range 8-12, pH 12 produces the highest intensity of Al-O-Al and pH 8 the lowest intensity, which means the higher the pH, the higher the rates of hydrolysis and crosslinking.

In Fig. 5, we show the FTIR spectra of sintered products obtained from precursor (Fig. 5a) and gel (Figs. 5b-5f). The spectral pattern of ceramic products obtained from precursor and gel in the frequency range 500-1200 cm^{-1} look very similar as evident by comparing Fig. 5a versus Figs. 5b-5f. All show initial spinel transformation at 700°C, but for the gels, at higher pH, 9-12, the FTIR spectra show a peak at 1080 cm^{-1} that is characteristic of α-Al_2O_3 and the intensity of this peak also increases with increasing pH.. In general, Al_2O_3 is commonly found in the form of γ-Al_2O_3. However, here the gel environment, apparently results in the formation of some α-Al_2O_3, which coexists with the γ-Al_2O_3 and $MgSO_4$ spinel.

XRD analysis was carried out following pyrolysis at temperatures between 700°C and 1300°C. The results are shown in Fig. 6. At lower pyrolysis temperatures, the spinel phase is a solid solution of $MgAl_2O_4$ and γ-Al_2O_3, but at higher temperatures the purity of the spinel phase increases (Fig. 6, using the ratio of the 400 hkl and 311 hkl reflections as indicator). At 1200°C, the gel formed at pH 8 transforms to a very high purity spinel (Fig. 6a). This temperature is below that used in other traditional methods such as solid-state reaction or co-precipitation.[10] The gels of higher pH also transform to a high purity spinel, but also contain a crystalline α-Al_2O_3 phase, as evidenced by the presence of diffraction peaks characteristic of α-

Al_2O_3 (Figs. 6b-6e). This may be due to a higher degree of crosslinking, which may obstruct molecular transport, making it difficult for local compositional heterogeneities to dissipate. The intensity of reflections characteristic of α-Al_2O_3 also increases with increasing pH of buffer, indicating that at higher pH, molecules prefered to segregate into α-Al_2O_3. This may reflect a pH dependent change in the selective hydrolysis of the metallic species[8]. At 1300°C, all traces of γ-Al_2O_3 have disappeared, as indicated by the ratio of the 400 hkl and 311 hkl reflections.

The SEM photographs show morphological evidence to compare with the XRD results. The sintered products obtained from gel at pH 8 and 9 form more perfect crystals, as shown in Fig 7b, 7c, which is consistent with the results of XRD. Actually, $MgAl_2O_4$ spinel belongs to the class of AB_2O_4 crystals, where the A and B cations are in the +2 and +3 oxidation state , which form a cubic structure. The Mg^+ ions exclusively occupy the tetrahedral sites and the Al^{+3} ions occupy the octahedral sites.[11] Hence, the sintered gel obtained from buffer of pH 8 shows individual cubic crystals as seen in Fig 7b. However, as shown in Fig 8, when the temperature is raised to 1300°C, SEM indicates that the crystals begin to fuse together, which is problematical since fusion affects the size and surface area of the particles. From the SEM data of Fig. 7, the gel sintered at 1200°C has individual particle sizes is about 5µm, whereas, from Fig. 8, the gel sintered at 1300°C had considerably larger particle size (~10 μm).

As shown in Figs 9a and 9b, SEM analysis of product sintered at 1200 °C from gels formed in buffer of pH 8 and 9 at 40°C shows less perfect crystallization, compared to the corresponding product from the same gels at 27°C (Figure 7). The explanation for this result is presumed to be that the higher temperature enhances the rates of hydrolysis and crosslinking. The increased reaction rate allows less time for the reactants to align themselves, hence less crystallization. In general, many factors influence the kinetics of hydrolysis (k_H) and condensation (k_C) because both processes occur simultaneously. The most important variables are temperature, nature and concentration of electrolyte, nature of solvent, and type of alkoxide precursor.[12-14]

The BET surface area, pore volume and pore size distribution of sintered products were obtained and are listed in Table I. Evidently, the specific surface area and average pore size of all samples differ significantly as evident. From table I, we see that increase of pH leads to an increase in surface area, pore volume and pore size, an exception occurring at pH 10. The reason for this anomaly is not clear, but it is interesting to note that, because of the presence of TEA, the pH of the system was actually about 10.70. The following reaction

$$MgO(s) + H_2O \longleftrightarrow Mg^{2+} + 2OH^-$$

is reported to reach equilibrium at pH 10.74 [15]. Thus, at this point, Mg prefers to form Mg^{2+} rather than form M-O bonds, as a result condensation reaction decreases, which may affect the microstructure of product.

The pore size distributions of all samples differ significantly, as shown in Fig10. From these plots, we can conclude that precursor which was subjected to sol-gel processing had a more homogeneous pore size distribution compared with that of the precursor sintered at the same temperature. The reason is believed to be that sol-gel processing allowed the molecular components to more uniformly reorganize during the heat treatment process. The sintered gel obtained from buffer pH 8 had a very narrow pore size distribution, which was further brought about because of the decreased rate of hydrolysis and condensation reaction.

The results of moisture absorption tests are shown in Table II. Products, which passed through the sol-gel process, had a higher capacity for moisture absorption. The sintered gel obtained from buffer pH 12 had a particularly high capacity which is consistent with the fact that it had high surface area and pore volume as evident in table I. From previous work [16-18], the humidity sensitivity is influenced by both total porosity and pore size distribution. Sintered gel obtained from buffer pH 8 had a lower surface area and pore volume compared to the precursor, but showed quite comparable moisture absorption, which further suggests that pore size distribution is a factor which enhances the absorption of water.

The sintered gel obtained from buffer of pH 10 had the lowest surface area and pore volume, but had a high capacity for moisture adsorption. Previous studies indicated that there is an optimum pore size of $MgAl_2O_4$ for humidity sensing, which was in the range 20-300 nm. Pores smaller than 20 nm and larger than 500 nm did

not seem to produce an effective response. From Fig. 10, we see that the sintered gel from buffer of pH 10 had a high percentage of pores in this size range and had a relatively uniform pore size distribution which is consistent with its high response.

Table II further indicates that, when the temperature rises, the capacity to adsorb water molecules decreases. To understand this, we must consider the water adsorption mechanism. Initially, when dry samples were exposed to high humidity, chemisorption of water on the oxide surface occured by a dissociative mechanism, principally at the neck regions of crystal grains. The water molecules adsorbed at metal cations on the surface, which generate a high local charge density and strong electrostatic field, and dissociate to form hydroxyl ions. In this step, higher temperature helped to overcome the activation energy. Subsequently, a layer of water molecules was physically adsorbed on the first hydroxyl layer, and dissociated to form H_3O^+ because of the high electrostatic fields.

The interaction between the pore structure of the spinel and water must also be considered. The porosity permits water condensation to occur by capillary action in the pores. The quantity of condensed water depends on the available pore sizes and their distribution. It is possible to estimate the pore radius at which capillary condensation occurs at a specified temperature (T) using the Kelvin equation:

$$r_k = \frac{2\gamma M}{\rho RT \ln (P_s/P)} \qquad (3)$$

where r_k is the Kelvin radius, P is the water-vapour pressure, P_s is the water-vapour pressure at saturation, γ and ρ are the surface tension (72.75 dyn.cm^{-1} at 20°C) and density, respectively. M is the molecular weight of water

Water condensation takes place in all pores with radii up to r_k. From the eq. (3), the smaller the radius or lower the temperature, the more easily condensation occurs [16-18]. Since from Table III, the amount of water adsorbed at 40°C was lower than that adsorbed at 27°C, evidently the uptake of water was controlled by the influence of capillary condensation.

It follows that physisorption of water molecules plays a key role in the effectiveness of this type of humidity sensor, which can operate at low temperature (< 100°C), and can be made using many ionic ceramics. High surface area, high pore

volume and homogeneous pore size distribution are the microstructural features that are key for optimal humidity sensing materials.

Sol-gel transition

It is of interest to investigate the effect of solvent conditions on the kinetics of the sol-gel process. This can be accomplished by carrying out rheological measurements during the gelation process. Specifically, we monitor the storage and loss dynamic moduli, $G'(\omega)$ and $G''(\omega)$, during gelation. At low frequencies, these quantities exhibit a power law dependence on frequency of deformation:

$$G'(\omega) = A\omega^{n'} \quad (4) \quad \text{and} \quad G''(\omega) = B\omega^{n''} \quad (5)$$

The gel point is located[19,20] by the fact that G' and G'' exhibit an identical frequency dependence, i.e. n' = n'', which corresponds to a frequency- independent loss tangent,

$$\tan\delta = G''/G' \quad (6)$$

A typical experiment is illustrated in Fig. 11. As the cross-linking reaction proceeds, the exponents n' and n'' decrease and exhibit a crossover at the gel point, where $n' = n'' = n^{(19,20)}$. A further characteristic is that $\tan\delta$ becomes independent of the frequency of deformation as shown in Fig. 11b, and moreover, there is a dramatic increase in the dynamic viscosity η^*, as illustrated in Fig 11c. In the sol state, η^* is small and frequency-independent, indicative of a Newtonian fluid, after the gel point η^* is large at low frequencies, and strongly decreases with frequency, indicative of a viscoelastic solid (i.e. a gel).

Table II summarizes the gelation times measured under different solvent conditions and temperatures. We see that the gel obtained from buffer of pH 8 exhibits the longest gelation times at both temperatures, which corresponds to the slowest rate of hydrolysis, as confirmed by FTIR analysis (Figure 4), and hence the slowest rate of cross-linking. Increase of pH and increase of temperature, means more rapid hydrolysis and crosslinking, and shorter gel times. These results yield further insight into the observation that the rate of hydrolysis and associated crosslinking reactions influences the microscopic organization of the gel and hence the sintered gel product, evidenced by the FTIR, XRD and SEM results described above. Higher pH and higher temperature lead to higher hydrolysis rates, which

provide less time for the molecules to redistribute, leading to local heterogeneities, i.e. the presence of a $MgSO_4$-γ-Al_2O_3 solid solution at lower sintering temperatures, an α-Al_2O_3 phase, and less perfect crystallization. Evidently, pH and temperature can be manipulated to alter the rate of hydrolysis and crosslinking of the gel, and hence control the microstructure of the sintered product.

Conclusions

The optimal sintering temperature needed to transform the $MgAl_2O_4$ double alkoxide precursor, prepared using the OOPS process, into spinel is 1200°C. Below this temperature, a pure spinel phase requires long annealing times, above this temperature, the spinel crystals fuse. This temperature is lower than that required in alternative synthesis routes (1500°-1600°C), and the spinel product obtained is of higher purity.

Sol-gel processing strongly influences the microstructure and morphology of sintered product. With the precursor concentration fixed at 20% (w/v), gel formed in buffer of pH 8 produced a spinel with very narrow pore size distribution, and buffer pH 12 produced a heterogeneous product, however, with, however, the highest surface area and pore volume and the highest level of moisture absorption. Moreover, most sintered gels exhibit higher moisture absorption compare to sintered product directly from the precursor. Levels of moisture absorption as high as 0.31 (g H_2O/g sample) can be obtained.

References

1. Laine, R. M., Mueller, B. L., and Hinklin, T., U. S. Patent No. 5,418,298, May 23, 1995.

2. Waldner, K.F., Laine, R.M., Dhumrongvaraporn (Wongkasemjit), S., Tayaniphan, S., and Narayanan, R. "Synthesis of double alkoxide precursor to spinel ($MgAl_2O_4$) directly from $Al(OH)_3$, MgO, and triethanolamine and its pyrolytic transformation to spinel", *Chemistry of Materials*, 1996, 8, No.12, 2850-2857.

3. Bickmore, R.B., Waldner, K.F., Laine, R.M, and Treadwell, D.R, "Ultrafine spinel powders by flame spay pyrolysis of a Magnesium Aluminum Double Alkoxide", *J.Am.Ceram.Soc.*, 1996, 79, No.5, 1419-1423.

4. Nitta, T., "Ceramic humidity sensor", *American Chemical Society*, 1981, 20, No.4, 669-674.

5. Gusmano, G., Gnappi, G., Montenero, A., and Traversa, E., "Microstructure and electrical propperties of $MgAl_2O_4$ thin films for humidity sensing", *Br. Ceram.Trans.*, 1996, 92, No.3, 104-108.

6. Traversa, E., Gnappi, G., Montenero, A., and Gusmano, G., "Ceramic thin films by sol-gel processing as novel materials for integrated humidity sensors", *Sensors and Actuators B*, 1996, 31, 59-70.

7. Laobuthee, A., Wongkasemjit, S., Traversa, E., and Laine, R.M., "$MgAl_2O_4$ spinel powders from oxide one pot synthesis process (OOPS) for ceramic humidity sensors", *J.of the European Ceramic Society*, 2000, 20, 91-97.

8. Julien,P., Mireille, R.P., and serge, V. , "Influence of the sol-gel synthesis on the formation of spinel $MgAl_2O_4$", *Material Research Bulletin*, 1998, 33, No.11, 1717-1724.

9. Pasquire, J.F., Komaneni, S., Roy, R.J., " Synthesis of $MgAl_2O_4$ Spinel : Seeding Effect on Formation Temperature", *J.Mater.Sci.*, 1991, 26, 3797-3802.

10. Reed, J.S., *Introduction to the principles of ceramic processing*, John Willey and Sons, New York, 1989.

11. Barsoum, M.W., *Fundamentals of ceramics*, The McGraw-Hill Companies, London, 1997.

12. Othmer, K., *Encyclopedia of Chemical Technology*, 4th ed,, John.Wiley and sons, New York, 1997.

13. Ertl, G., Knozinger, H. and Weitkamp, J., *Handbook of Heterogeneous Catalysis*, 1997.

14. Ram, C.M., "Metal alkoxides and theirs derivatives with carboxylic acids and diketones as precursors in solution sol-gel process", *Sol-Gel Science and Technology*, 1989, 40-60.

15. Lower, S.K., *A chemI Reference Text*, Simon Fraser University, 2000.

16. Gusmano, G., Montesperelli, G., Nunziante, P., and Traversa, E., "The electrical behavior of MgAl$_2$O$_4$ pellets as function of relative humidity", *Materials Engineering,* 1992, 3, No.3, 417-434.

17. Gusmano, G., Montesperelli, G., Nunziante, P., and Traversa, E., " Study of the conduction mechanism of MgAl$_2$O$_4$ at different environmental humidities", *Electrochimica Acta,* 1993, 38, No.17, 2617-2621.

18. Traversa, E., "Ceramic sensors for humidity detection : the state-of-the-art and future developments", *Sensor and Actuators B*, 1995, 23, 135-156.

19. Winter, H.H., Chambon, F., "Analysis of linear viscoelasticity of a cross-linking polymer at the gel point", J. Rheol., 30, 1986, 367-382.

20. Hsu, S. H. and Jamieson, A. M., "Viscoelastic studies of the sol-gel transition of gelatin", Polymer, 1993, 34, 2602-2608.

CAPTIONS OF TABLES AND FIGURES

Figure 1. Structure of $MgAl_2O_4$ double alkoxide precursor produced by the OOPS process.

Figure 2. FTIR spectrum of $MgAl_2O_4$ double alkoxide precursor

Figure 3. XRD pattern of $MgAl_2O_4$ double alkoxide precursor after sintering at various temperatures shown. The 311 and 400 peaks used to assess purity of the spinel phase are identified.

Figure 4. Time evolution of the FTIR spectrum of $MgAl_2O_4$ precursor during the hydrolysis reaction as a function of pH:

(a) precursor   (b) pH 8   (c) pH 9   (d) pH 10   (e) pH 11   (f) pH 12

Figure 5. Effect of pH and sintering temperature on the FTIR spectrum of ceramic product:

(a) pH 8   (b) pH 9   (c) pH 10   (d) pH 11   (e) pH 12

Figure 6. Effect of pH and temperature on the crystal structure of ceramic product:

(a) pH 8   (b) pH 9   (c) pH 10   (d) pH 11   (e) pH 12

Figure 7. SEM photographs of ceramic product sintered at 1200°C following sol-gel processing at 30 °C:

(a) precursor (b) pH 8   (c) pH 9   (d) pH 10   (e) pH 11   (f) pH 12

Figure 8. SEM photographs of ceramic products sintered at 1300 °C following sol-gel processing at 30 °C:

(a) pH 8   (b) pH 9   (c) pH 10   (d) pH 11   (e) pH 12

Figure 9. SEM photographs of ceramic products sintered at 1200 °C following sol-gel processing at 40 °C:

(a) pH8   (b) pH9

Figure 10. Pore size distribution of ceramic products sintered at 1200°C:

(a) precursor (b) pH8   (c) pH10 (d) pH 12

Figure 11. Rheological charcterisation of the sol-gel transition of $MgAl_2O_4$ precursor dissolved in buffer of pH 9:

(a) n' and n" vs. time   (b) tanδ vs. time   (c) η^* vs. time

Table I   BET Analysis of Ceramic Products

$$MgO + 2Al(OH)_3 + x'EG$$

$200°C/7\ hr. \qquad \downarrow \qquad -H_2O$

Figure 1.

Absorbance Units

Wavenumber cm^{-1}
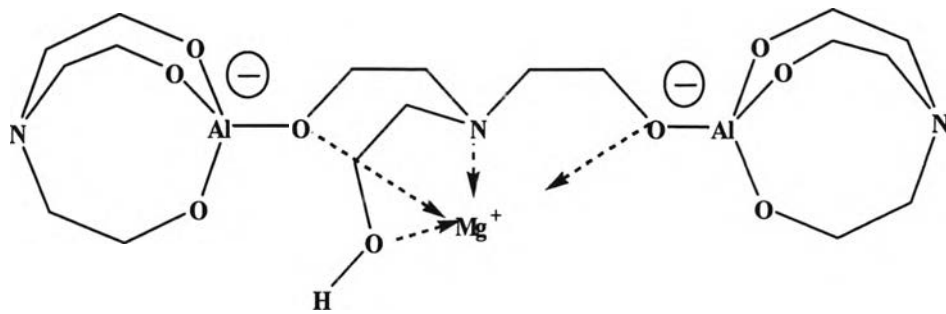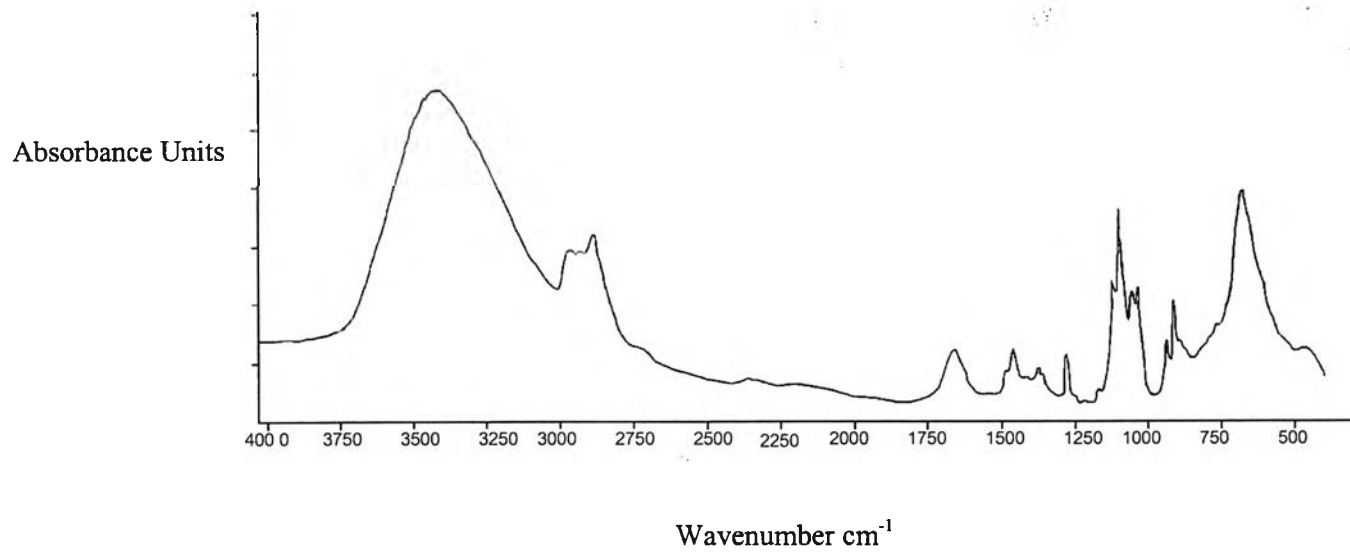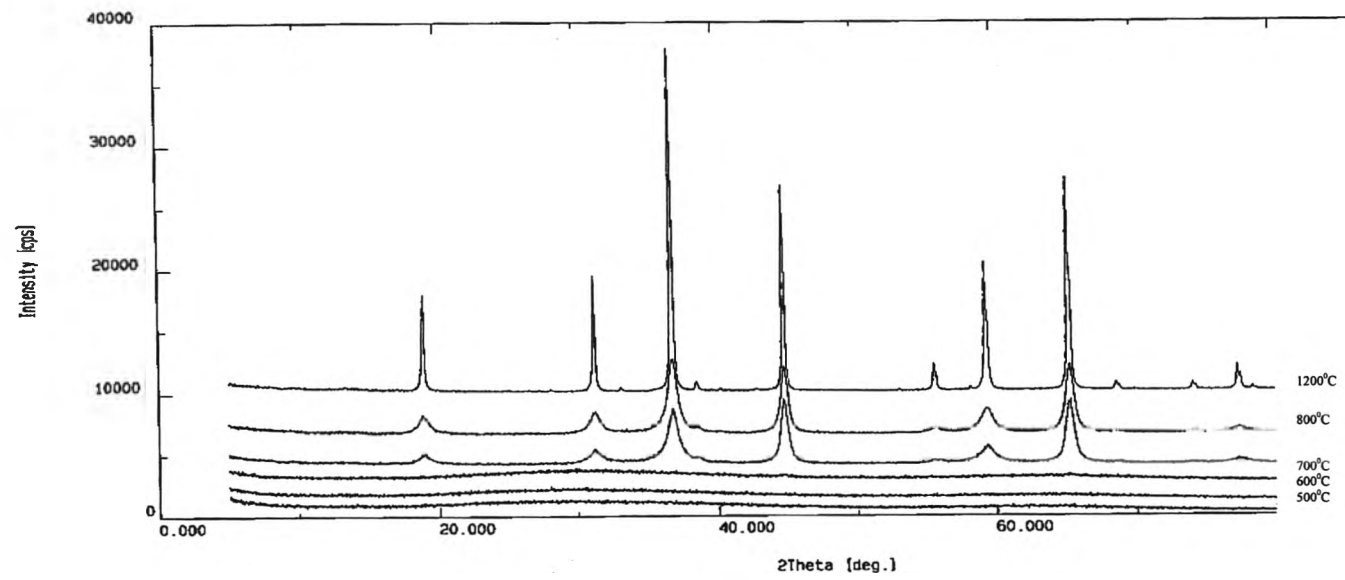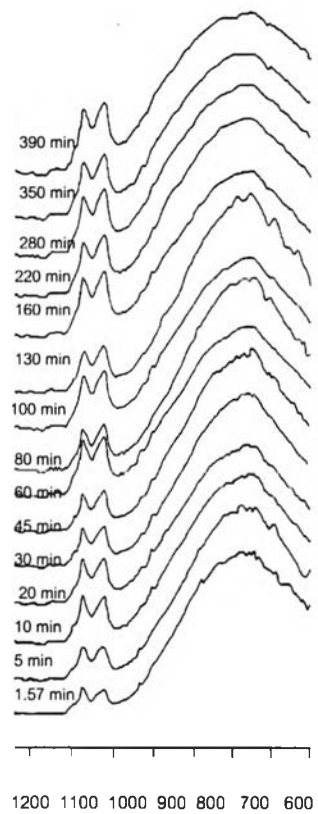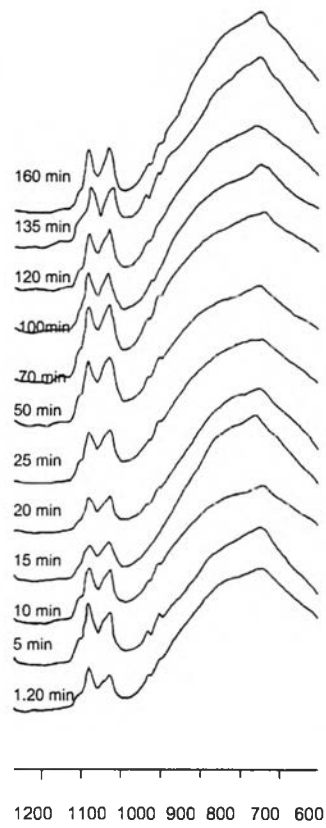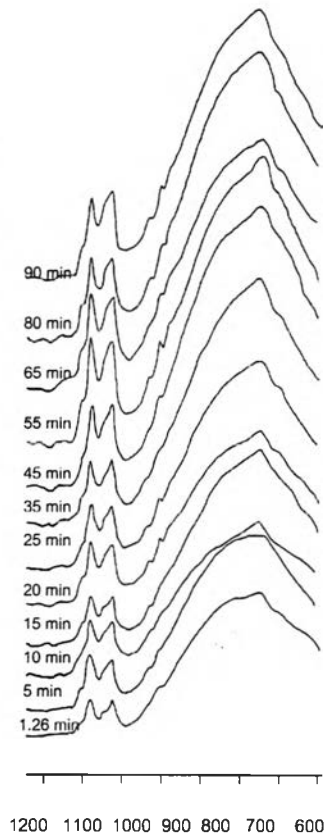
Figure 2.
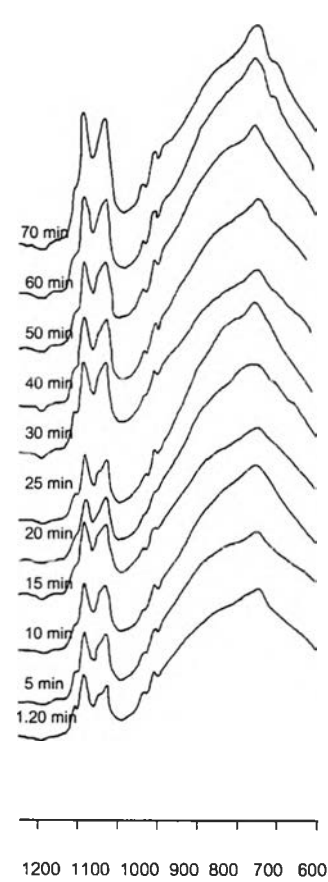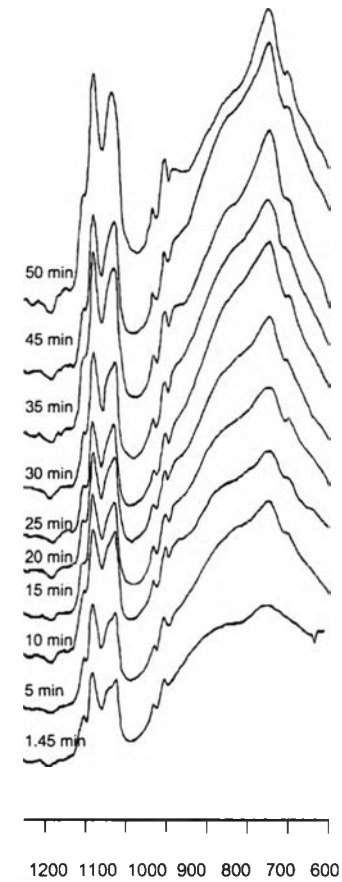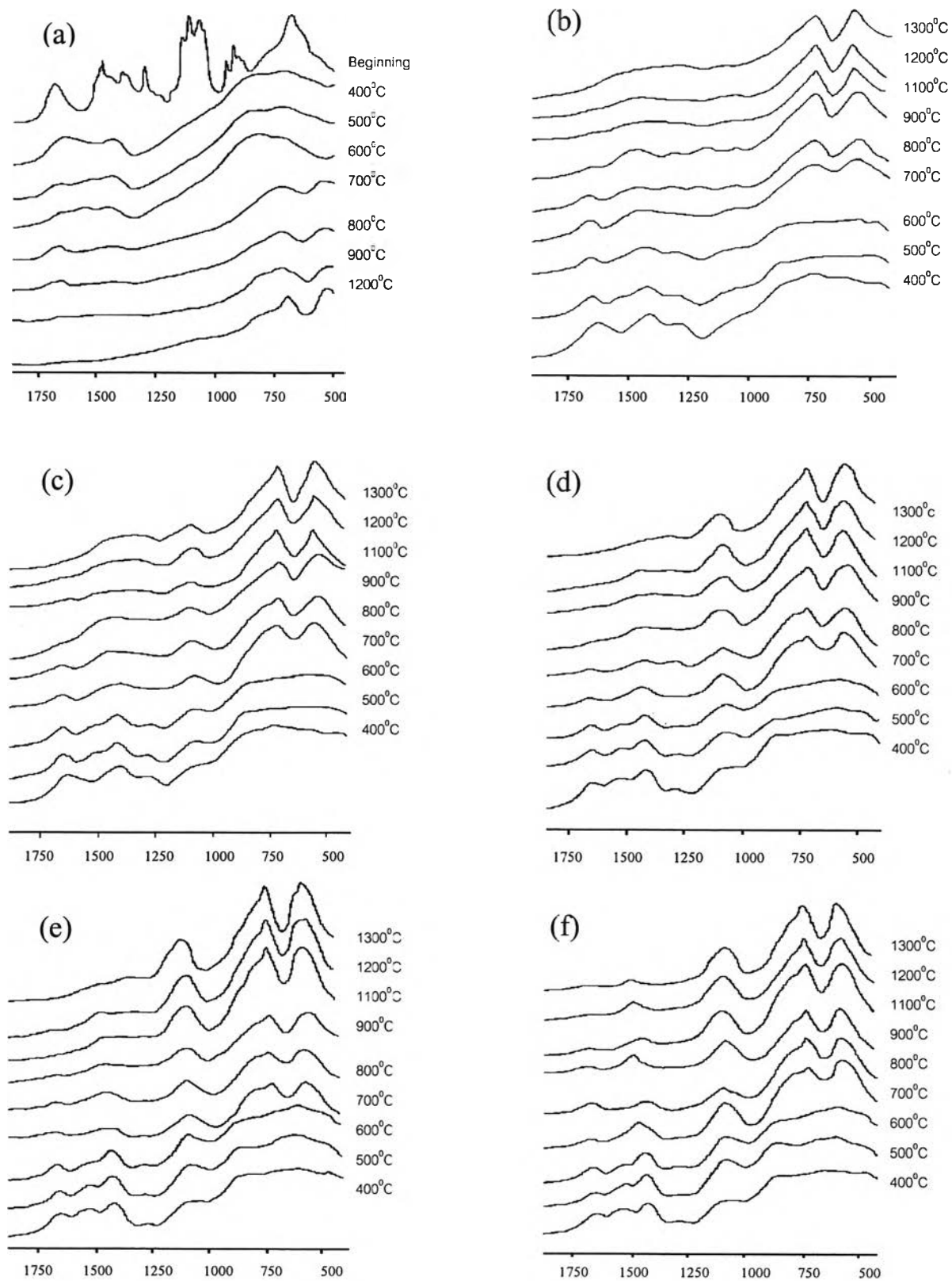
Figure 3.
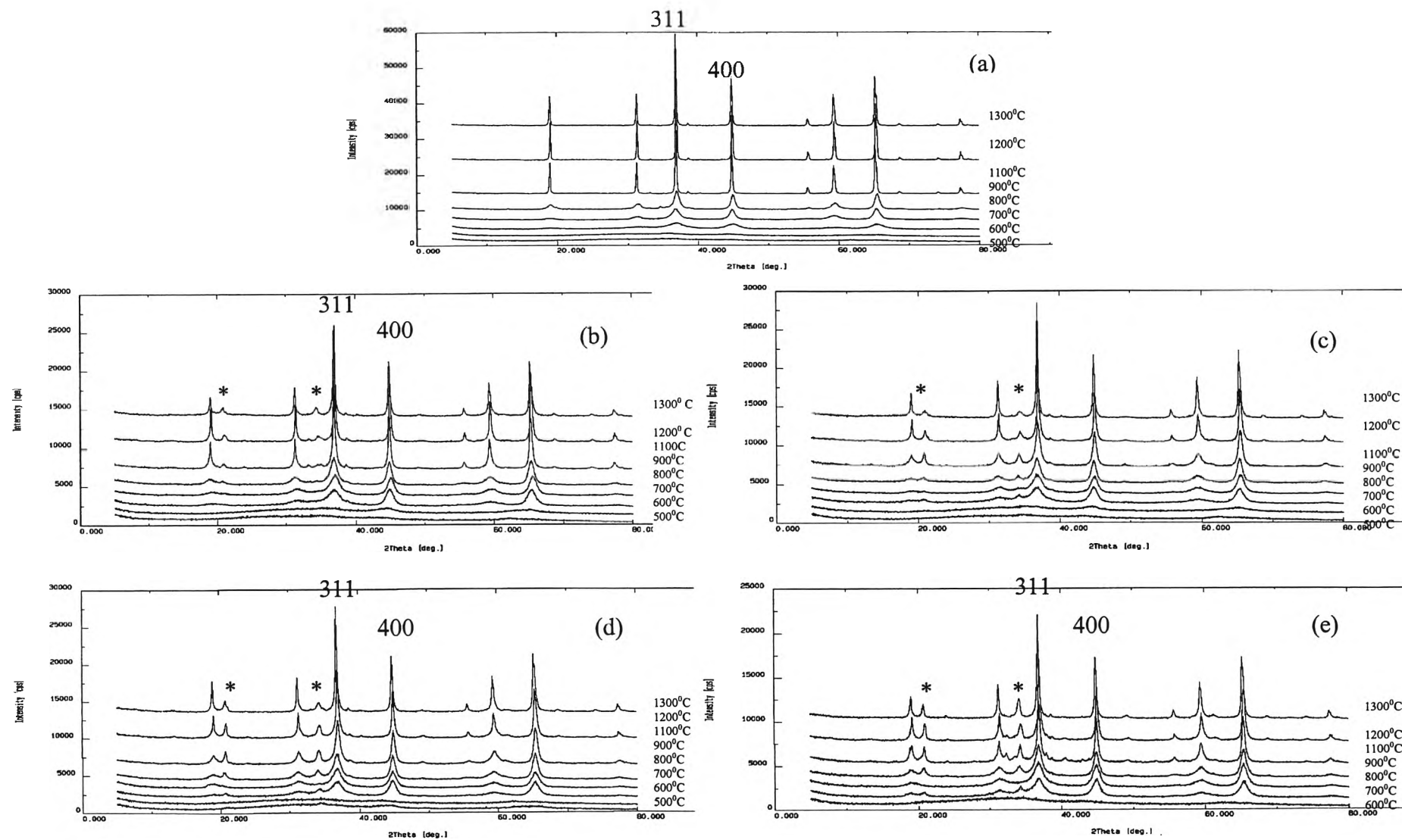
Figure 4.

Figure 5.

Figure 6

* α-Al₂O₃
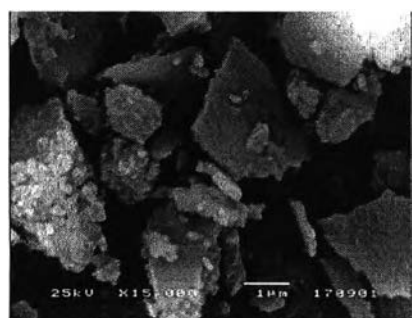
(a)
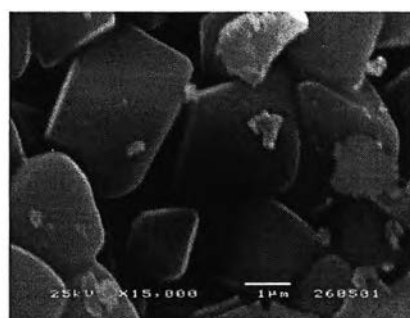
(b)
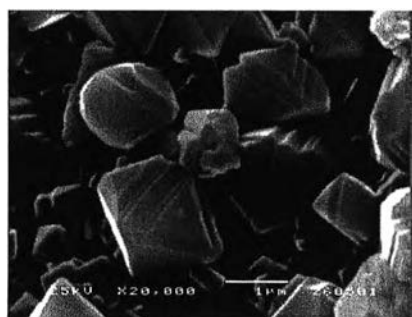
(c)
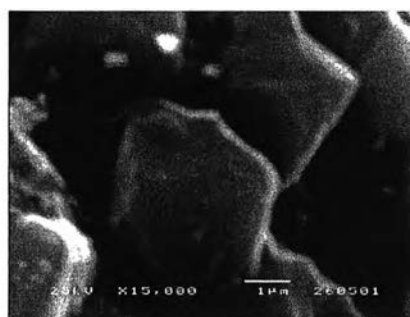
(d)
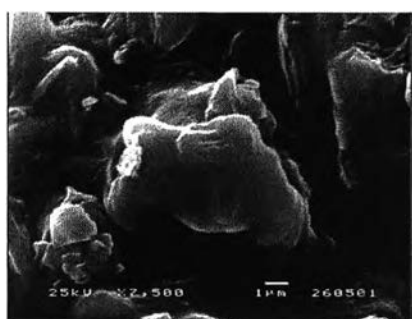
(e)

(f)
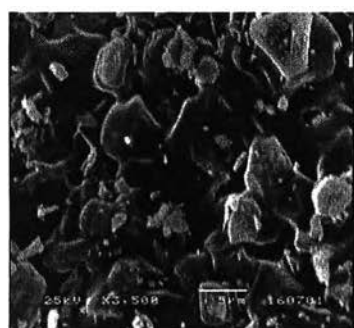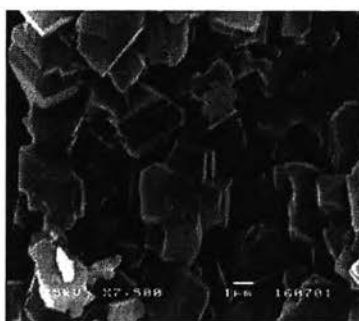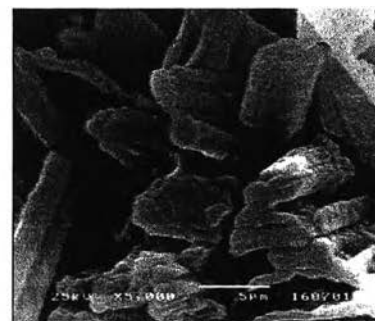
Figure 7.

(a)　　　　　　　　　(b)　　　　　　　　　(c)

Figure 8.
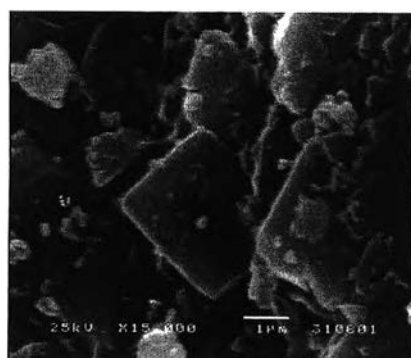
(a)

(b)

Figure 9.
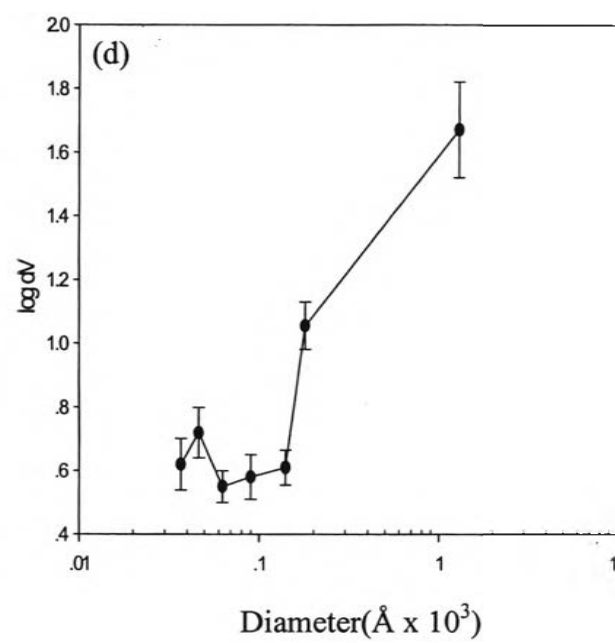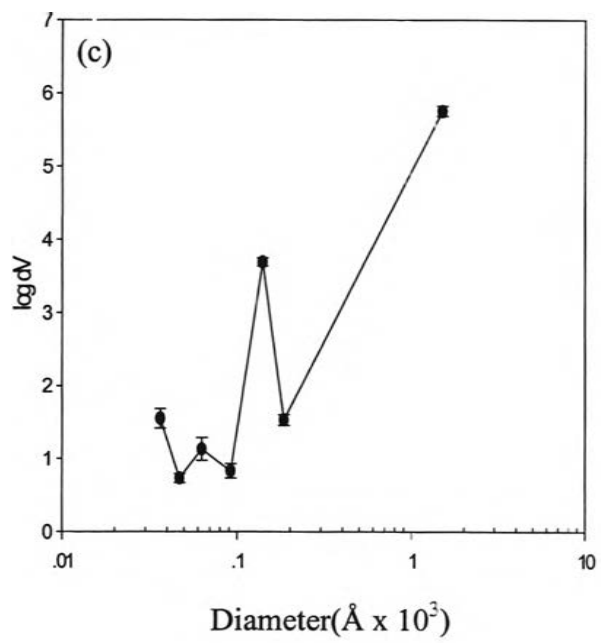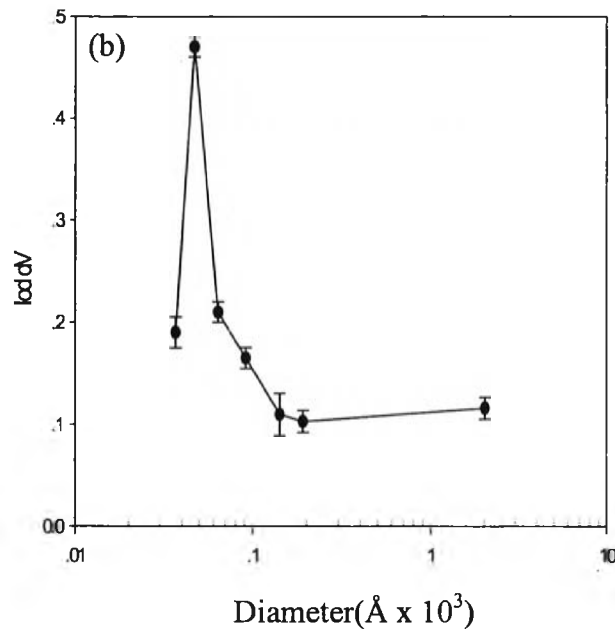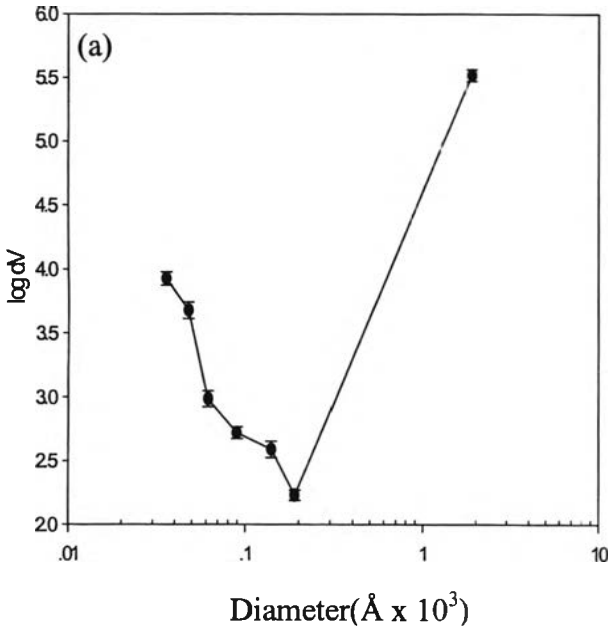
Figure 10

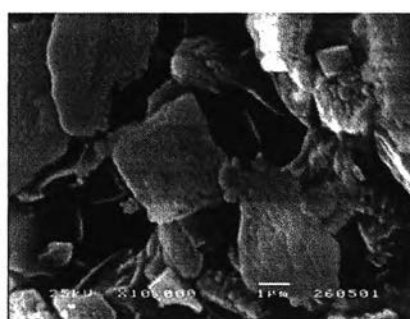**Figure 11a.**

tanδ

Time (s)
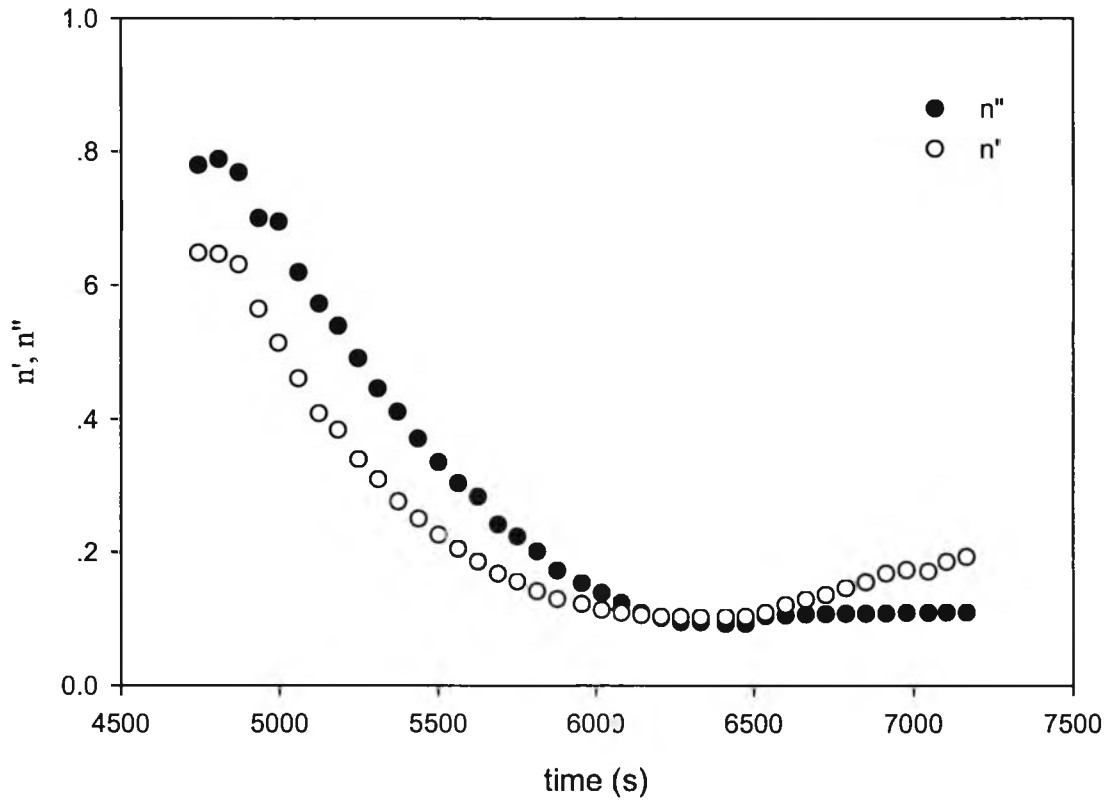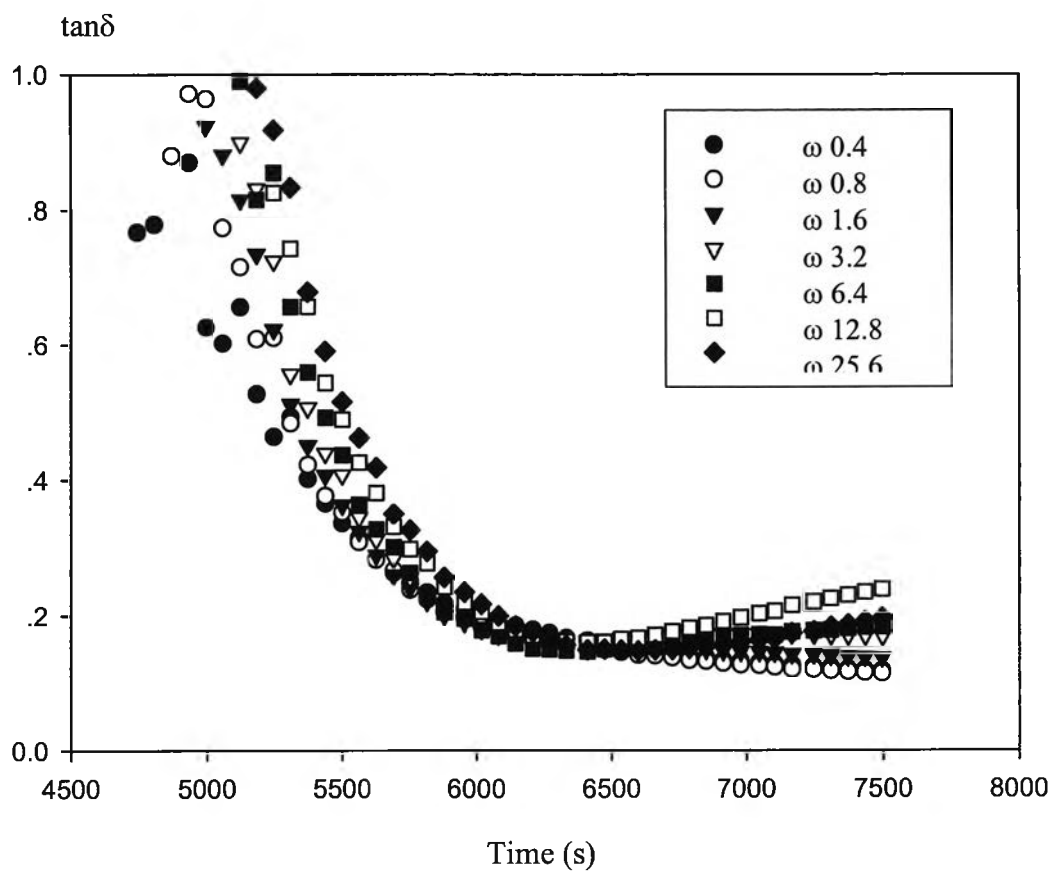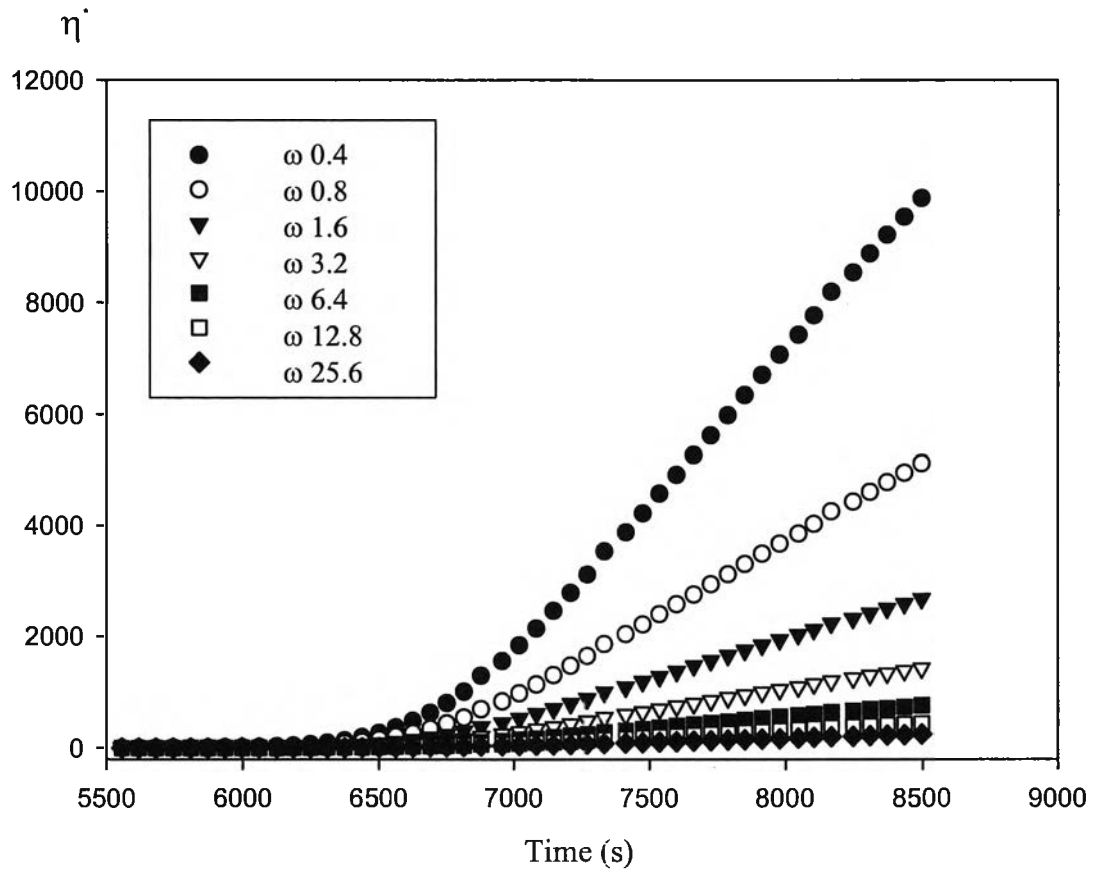
Figure 11b.

Figure 11c.

Condition	Surface area (m^2/g)	Mesopore area (m2/g)	Micropore area (m2/g)	Pore volume (cc/g)(x 10^{-3})	pore size (Å)
Precursor	2.840	2.840	2.858	2.951	41
pH 8/27°C	1.773	1.773	2.823	1.80	40
pH 9/27°C	2.097	2.097	2.823	2.111	40
pH 10/27°C	1.488	1.488	1.137	1.648	44
pH11/27°C	3.136	3.136	1.887	3.599	45
PH12/27°C	5.295	5.295	2.178	6.16	46
pH8/40°C	1.202	1.202	1.764	1.060	35
pH9/40°C	2.034	2.034	2.489	2.102	41

Table I.

pH /Temperature (°C)	27°C (g H$_2$O/g sample)	40°C (g H$_2$O/g sample)
Precursor	0.05	0.01
8	0.03	0.02
9	0.13	0.11
10	0.31	0.22
11	0.29	0.26
12	0.30	0.31

Table II.

pH	Gelation time (s)
8 at 27°C	19280
9 at 27°C	6240
10 at 27°C	2400
11 at 27°C	971
12 at 27°C	810
8 at 40°C	2580
9 at 40°C	740

Table III.